Proceedings of the International School-seminar
"New Physics and Quantum Chromodynamics at external Conditions", pp. 27 – 37,
3-6 May 2007, Dnipropetrovsk, Ukraine

TOPOLOGY, CENTER VORTICES, CONFINEMENT AND CHIRAL SYMMETRY BREAKING IN SU(2) LATTICE QCD

Manfried Faber, Gerald Jordan and Roman Höllwieser

Atominstitut der Österreichischen Universitäten,
Vienna University of Technology,
Wien, Austria

1 Introduction

The fact that lattice QCD is able to describe confinement and chiral symmetry breaking is known since a long time. Actually, one of the pioneering papers of Mike Creutz [1] was already showing that the potential between static quarks and antiquarks is asymptotically linear rising with the distance. The corresponding constant force, the string tension, is incredible high, around 1 GeV/fm. The origin of this strong force should be found in the properties of the QCD vacuum. This is highly non-trivial, filled with quantum fluctuations and topological excitations which dominate the behaviour of the QCD vacuum at long distance scales. On the other hand the color electric field between quarks and antiquarks has regular flux lines and does not like to enter the stochastically fluctuating QCD vacuum. Therefore, it is energetically favourable to compress the electric flux-lines to a small tunnel between quark and antiquark. The distribution of these colour magnetic flux was nicely shown in lattice calculations [2]. Despite intensive efforts over three decades there is no derivation of confinement from first principles nor is there a generally accepted explanation. Candidates for topological excitations responsible for confinement were mainly instantons, abelian monopoles and vortices. Instantons live on a length scale of around 0.2 fm and can therefore contribute only little to the large distance force between heavy quarks [3].

By a transformation to the dual degrees of freedom one can show analytically that confinement in U(1) lattice gauge theory is due to magnetic monopoles. Kronfeld, Schierholz, and Wiese [4] devised a method for non-abelian gauge theories to detect monopoles by abelian gauge fixing and abelian projection. The property that an abelian component of the colour field can explain the full string tension was shown by [5] and was dubbed Abelian dominance. The monopole confinement mechanism leads to a very nice picture, the dual superconductor model of confinement, where magnetic monopoles and antimonopoles form a solenoidal current around the electric flux tube between quark and antiquark. But in ref. [6] we could show that the hypothesis of Abelian dominance in the maximal Abelian gauge, which was known to work for Wilson loops in the fundamental representation, fails for Wilson loops in higher group representations. Such a problem does not appear in the center vortex picture of confinement.

Center vortices are closed magnetic flux lines which carry flux corresponding to the center of the gauge group. The vortex model was first proposed by 't Hooft [7], Mack and Petkova [8] and [9]. Due to lack of an identification method for vortices, almost no numerical investigations were done for 25 years. Maximal center gauge and center projection gave us means to identify vortices[10] and led to new investigations using the vortex model. The central idea was to filter out the important infrared degrees of freedom responsible for confinement and then to simplify the field configurations by projection. Other identification methods for vortices were proposed, Laplacian center gauge by de Forcrand and coworkers [11, 12], a method by Langfeld it et al. [13] which combines Laplacian center gauge and direct maximal center gauge, and direct Laplacian center gauge [14]. All of the center gauges yield qualitatively similar results. The most important achievements are

- **Center dominance**. The vortices in the projected Z(2) gauge theory, the so called projected or P-vortices reproduce a good deal of the string tension of the full Yang-Mills theory, see Fig. 1 [14]. A removal of the P-vortices from the lattice configuration results in a loss of the confining properties [14] as depicted in Fig. 2.
- **Precocious linearity**. The projected potential is already linear at two lattice spacings [14], see Fig. 3.
- **P-vortices locate thick center vortices**. Vortex limited Wilson loops W_n are expectation values of Wilson loops in the subensemble of those configurations where the minimal area of the loop is pierced by precisely n P-vortices. As shown in Fig. 4 for large loop area W_n approaches the limit $(-1)^n W_n$.

in cooperation with Roman Bertle, Michael Engelhardt, Jeff Greensite, Urs Heller and Stefan Olejnik

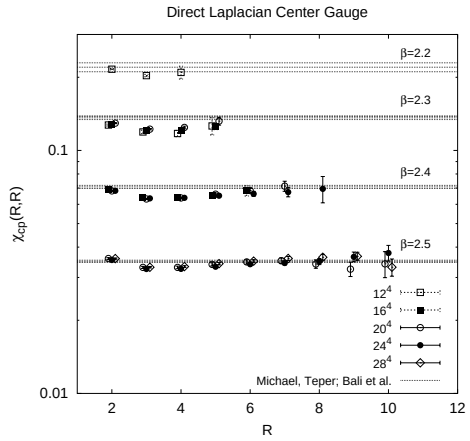

Figure 1. Center-projected Creutz ratios at $\beta = 2.2 - 2.5$ obtained after direct Laplacian center gauge fixing. Horizontal bands indicate the asymptotic string tensions on the unprojected lattice, with the corresponding errorbars [14].

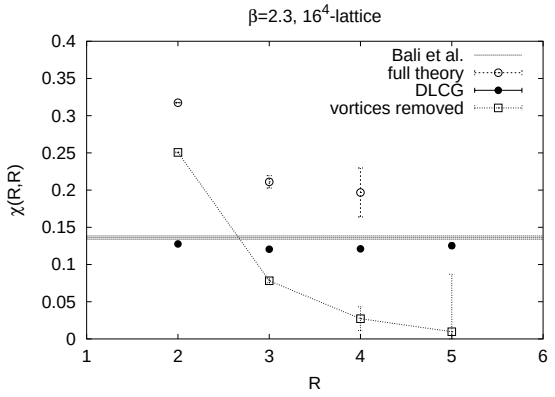

Figure 2. Creutz ratios on the modified lattice, with vortices removed, at $\beta = 2.3$. For comparison, we also display the unprojected Creutz ratios (open circles), the center projected Creutz ratios (solid circles), and the asymptotic string tension (horizontal band) [14].

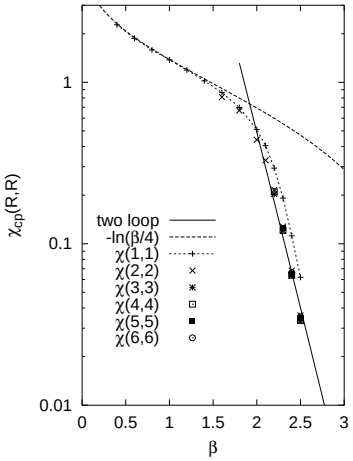

Figure 3. Creutz ratios from center-projected lattice configurations, in the direct Laplacian center gauge.[14]

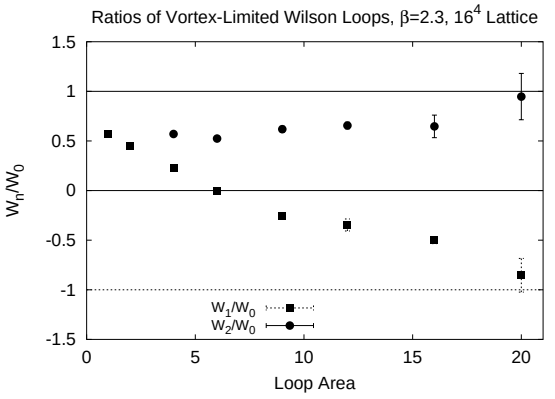

Figure 4. W_n/W_0 ratios at $\beta = 2.3$.[14]

- **Scaling of vortex density**. This was first observed by Langfeld *et al.* [15] and can also be seen in Fig. 3.

- **Finite temperature**. The P-vortex density across the deconfinement phase transition was first carried out by Langfeld *et al.* [16] and Chernodub *et al.* [17]. At zero temperature vortices are unoriebtable surfaces and percolate through the lattice [18]. At finite temperature P-vortices exist also in the deconfined phase. They form cylindric objects which extend in time direction, see Fig. 5. This explains the area law for space-like Wilson loops and the perimeter law for time-like Wilson loops.

- **Casimir scaling**. The asymptotic string tension depends on N-ality of the color charge only, so that for SU(2) $\sigma_j = \sigma_{1/2}$ for j half-integer $\sigma_j = 0$ for j integer there is still an intermediate range of distances where Casimir scaling applies (at least approximately), i.e. for SU(2) $\sigma_j = \frac{1}{2}j(j+1)$. We could show by a very simple ansatz [19] that for charge distances comparable to the thickness of these vortices the proportionality of the string tensions to the eigenvalue of the quadratic Casimir operator is very natural in a thick vortex model (Fig. 6). For distances large compared to the vortex thickness the string tension reduces to that of the thin vortex model.

- **Topological charge**. The vortex world-surfaces allow to determine the topological charge of configurations. This was first discussed in the continuum by Cornwall [35, 36], Engelhardt and Reinhardt [37] and then on the lattice in ref. [38]. The topological charge arises at lattice sites at which the tangent vectors

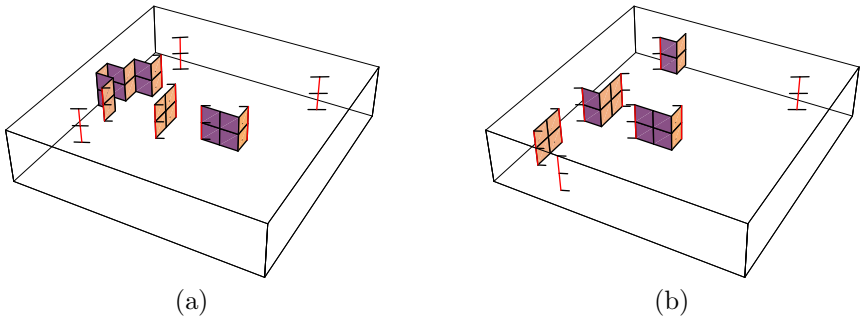

Figure 5. Dual P-plaquettes in a typical field configuration at $\beta = 2.6$, on a $2 \cdot 12^3$-lattice. Two successive z-slices for the x-y-t-subspace are shown. The amputated lines leaving the left figure towards right arrive in the right figure from the left.[18]

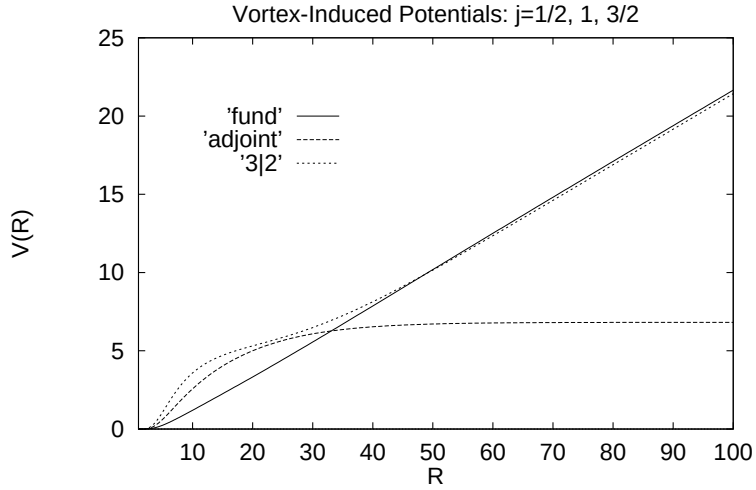

Figure 6. Interquark potential $V(R)$ induced by center vortices, according to the thick vortex model discussed in the text, for quark charges in the in the $j = \frac{1}{2},\ 1,\ \frac{3}{2}$ representations.[19]

to the vortex surface span all four space-time directions. Such sites are either self-intersections points or writhing points, see Fig. 7.

- **Relation to monopole confinement**. Vortices carry colour magnetic flux, after Abelian projection this flux appears as a monopole-antimonopole chain, as indicated schematically in Fig. 8 and discussed in ref. [19].

- **Vortices and matter fields**. Matter fields lead to a breaking of the gluon string. The interesting question how matter fields influence vortices was first studied in the SU(2)-Higgs model in the continuum in refs. [20, 21] and then on the lattice in [22–24].

2 Vortices and chiral symmetry breaking

Concerning chiral symmetry breaking a remarkable result was found by Forcrand and d'Elia[35], removing vortices from lattice configurations leads to restoration of chiral symmetry.

That smooth vortex configurations give rise to zero-modes of the Dirac operator was shown first in analytical calculations by the Tbingen group [26]. The zero-modes of the Dirac operator tend to peak at the intersections as shown in Fig. 10. These plots show the probability density of the zero-mode in a background of two pairs of intersecting vortex sheets.

Using the chirally improved Dirac operator Gattringer and the Tbingen group[27, 28] have investigated the influence of center vortices on the properties of the Dirac spectrum. They have shown, see Fig. 11, that the removal of center vortices eliminates the zero-modes and near-zero modes of the Dirac operator impliying via the Banks-Casher relation the restoration of chiral symmetry.

It was not understood why the spectra of the center projected configuration, the left diagram in Fig. 11, has developped a large gap indicating chirally symmetric field configurations. This is a very interesting result. It is up to now the only case where confinement does not lead to chiral symmetry breaking.

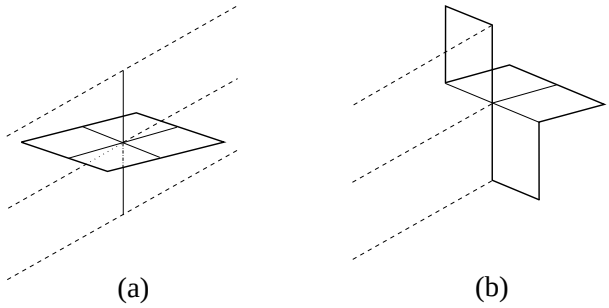

Figure 7. Intersection points (a) and writhing points (b) which contribute to the topological charge of a P-vortex surface. The full lines are space-like and the dashed lines time-like.

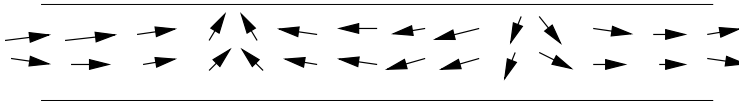

Figure 8. Vortex field strength after maximal abelian gauge fixing. Vortex strength is mainly in the horizontal $\pm s_3$ direction.

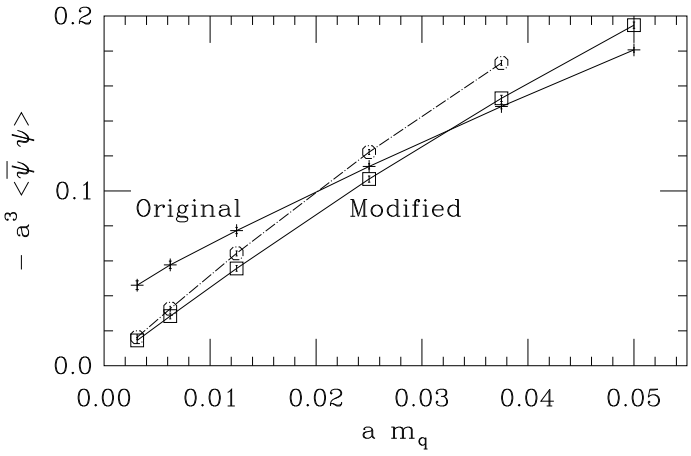

Figure 9. Chiral condensate in quenched lattice configurations before ("Original") and after ("Modified") vortex removal. From de Forcrand and D'Elia, ref.[35].

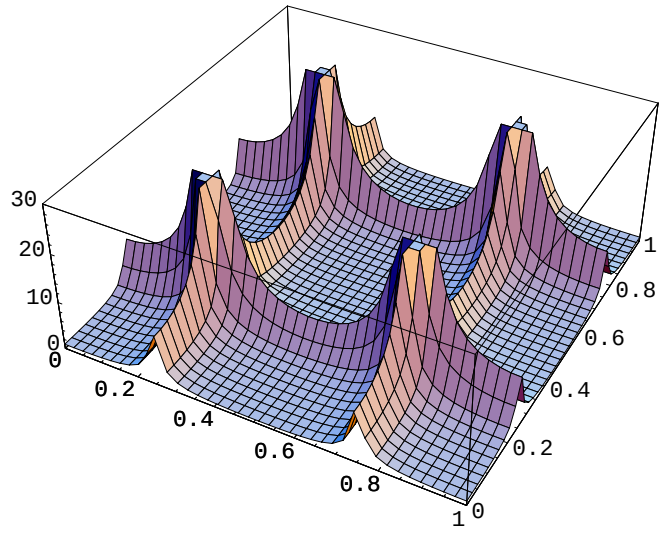

Figure 10. Probability density of the zero-mode in the background of four intersecting vortex sheets is shown in the two-dimensional subspace defined by the intersection points.[26]

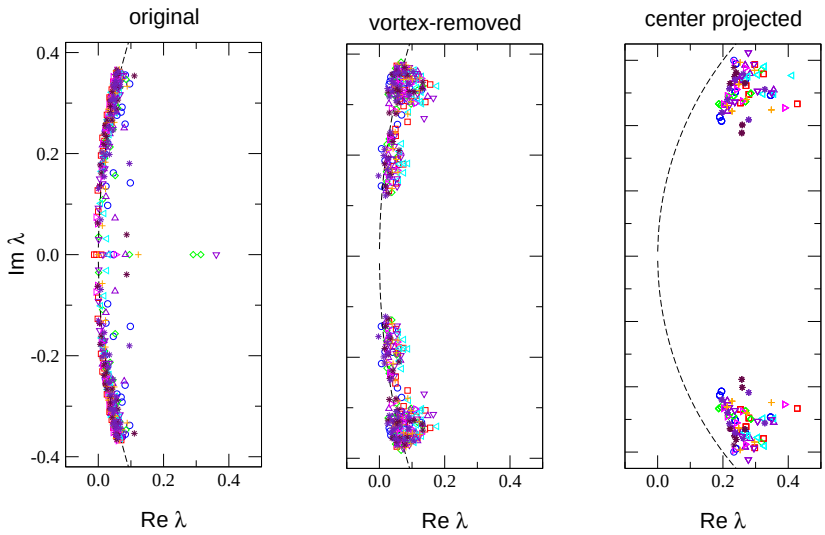

Figure 11. The 50 smallest Dirac eigenvalues from 10 different configurations are shown in the complex plane. The spectrum for the original ensemble (lhs. plot) are compared to the spectrum for vortex-removed configurations (rhs. plot) and the spectrum of center-projected configurations.[28]

3 Dirac operator and exact chiral symmetry

The chiral condensate

$$\bar{\psi}\psi = \bar{\psi}_l\psi_r + \bar{\psi}_r\psi_l \tag{1}$$

is the order parameter which indicates whether chiral symmetry is present or broken. In the chiral symmetric phase the phase transformations between right and left-handed quarks are independent and average $\bar{\psi}\psi$ to zero. In the chirally broken phase transformations of left handed quarks lead to phase changes of right handed quarks and result in $\bar{\psi}\psi \neq 0$. Lattice calculations indicate that a transition from the confined to the quark-gluon plasma phase is associate with a transition from the chirally broken to the chiral symmetric phase. This indicates that both phenomena, confinement and dynamical chiral symmetry breaking may have the same origin. Due to the strong indications that vortices explain confinement it is very important to investigate the relation of vortices to chiral symmetry breaking.

The discretisation of fermions in lattice QCD is a hard problem. The reason for this difficulty lies in the celebrated no-go theorem of Nielsen and Ninomiya. It states that is impossible to fulfill at the same time the conditions: no doublers, locality, translational invariance and reality of the bilinear fermion action. The theorem comes from topological arguments and implies that formulating fermions on a space-time lattice one of these requirements has to be given up.

The Nielsen-Ninomiya theorem requires

$$\{D, \gamma_5\} = 0 \tag{2}$$

to make the fermion action invariant under the usual continuum chiral rotations

$$\psi' = [1 + ie^a T^a \gamma_5]\psi, \qquad \bar{\psi}' = \bar{\psi}[1 + ie^a T^a \gamma_5] \tag{3}$$

T^a acts here in flavour space , where the Dirac operator D is proportional to unity. An interesting way around this dilemma was discovered by Ginsparg and Wilson in 1982[29]. The Ginsparg-Wilson operators obeys

$$\{D, \gamma_5\} = 2aD\gamma_5 D, \tag{4}$$

the famous Ginsparg-Wilson relation, where a is the lattice constant. In the continuum limit $a \to 0$, this reduces to the usual chiral symmetry, so that actual physics is not affected. It was further shown that the Ginsparg-Wilson relation implies an exact symmetry of the fermion action[30], which may be regarded as a lattice form of an infinitesimal chiral rotation. Thus the Ginsparg-Wilson relation offers an exact chiral symmetry. The price to pay is that such operators are not ultralocal and therefore computationally very demanding.

The Overlap-Dirac operator [31, 32] is a solution of the Ginsparg-Wilson relation and hence a realisation of chiral symmetry on the lattice

$$D_{ov} = 1/2\left[1 + \gamma_5 \epsilon(H_L^+)\right] \tag{5}$$

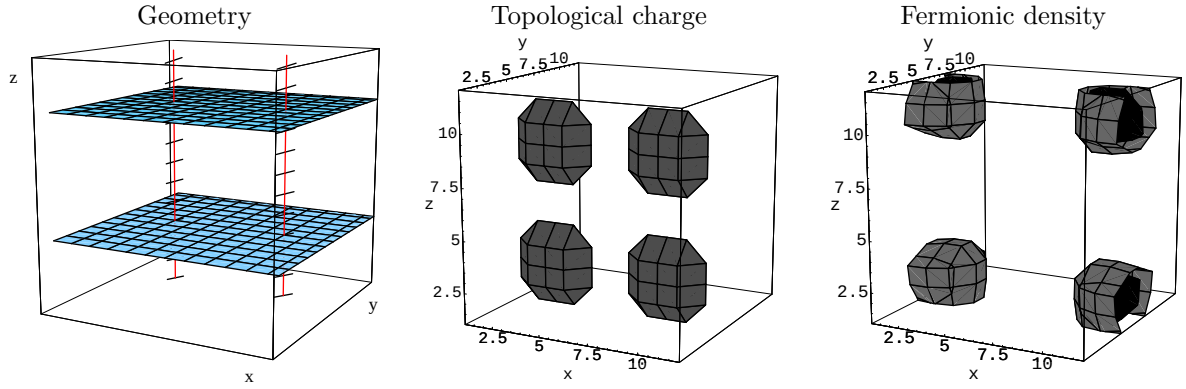

Figure 12. Two orthogonal pairs of plane vortices intersecting in four points

where ϵ is the matrix sign function

$$\epsilon(H) = H/\sqrt{H^2} \tag{6}$$

and

$$H_L^+ = \gamma_5 D_w(-\mu_0) \tag{7}$$

D_w is the usual lattice Wilson Dirac operator with $r = 1$

$$(D_w)_{x,y}(\mu) = -\frac{1}{2}\sum_\mu \left[(1+\gamma_\mu)U_\mu(x)\delta_{x+\hat{\mu},y} + (1-\gamma_\mu)U_\mu^\dagger(x-\hat{\mu})\delta_{x-\hat{\mu},y} - (\mu+4)2\delta_{x,y}\right] \tag{8}$$

The chirally improved fermions which were developed by Gattringer and Lang[33, 34] give an approximate solution of the Ginsparg-Wilson relation. The Dirac spectra shown in Fig. 11 were produced with chirally improved fermions. It is an interesting question whether the above mentioned failure to get chiral symmetry breaking from confing P-vortex configurations is a consequence of the approximation in the solution of the Ginsparg-Wilson relation or whether it is related to some missing properties of the projected vortices.

3.1 Atiyah-Singer index theorem and exact zero-modes

As mentioned above, the vortex world-surfaces allow to determine the topological charge [35–38]. By the Atiyah-Singer index theorem the topological index, the topological charge, is related to the analytical index, the number of exact zero-modes.

$$\text{ind}\, D[A] = n_- - n_+ = Q[A] \tag{9}$$

with n_-,n_+ number of left-/right-handed zeromodes. The axial anomaly

$$\gamma_\mu j_\mu^5 = -\frac{N_f}{16\pi^2}\text{Tr}\,(F_{\mu\nu}\tilde{F}_{\mu\nu}) \tag{10}$$

on the other hand gives upon inegration again the topological charge.

$$Q := \int d^4x \gamma_\mu j_\mu^5 \tag{11}$$

We localise the eigenvectors $\vec{v}$ for the zero-modes. Appropriate observables concerning the localisation are the scalar density

$$\rho(x) = \sum_{c,d} |\vec{v}(x)_{cd}|^2, \tag{12}$$

where the summation indices c and d refer to color und Dirac indices and further the chiral densities $\rho_+(x)$ and $\rho_-(x)$

$$\rho_\pm(x) = \sum_{c,d} \vec{v}(x)^*_{cd} \frac{1-\gamma_5^{c,d'}}{2} \vec{v}(x)^2_{cd'} \tag{13}$$

For plane vortices the number of intersection points and the Atiyah-Singer index theorem lead to the correct topological charge.

Besides plain vortices which are usually of abelian nature it is interesting to study non-abelian vortices which may have a spherical geometry. We distinguish between an orientable and a non-orientable spherical vortex.

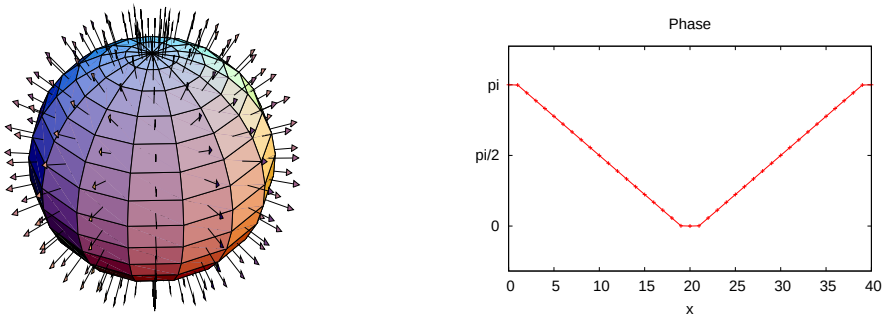

Figure 13. Thick Spherical SU(2)-vortex (hedgehog, non-orientable) and change of its link phase (α_-)

1. The non-orientable spherical vortex of radius R and thickness Δ is constructed with the following links:

$$U_\mu(x^\nu) = \begin{cases} \exp\left(\mathrm{i}\alpha(r)\vec{n}\cdot\vec{\sigma}\right) & t = 1, \mu = 4 \\ \mathbf{1} & \text{else} \end{cases} \tag{14}$$

$$\vec{n} = \vec{r}/r, \vec{r} = (x, y, z), \tag{15}$$

where the function α is either one from α_+, α_-, which are defined as

$$\alpha_+(r) = \begin{cases} \pi & r < R - \frac{\Delta}{2} \\ \frac{\pi}{2}\left(1 - \frac{r-R}{\Delta/2}\right) & R - \frac{\Delta}{2} < r < R + \frac{\Delta}{2}, \\ 0 & R + \frac{\Delta}{2} < r \end{cases} \qquad \alpha_-(r) = \begin{cases} 0 & r < R - \frac{\Delta}{2} \\ \frac{\pi}{2}\left(1 + \frac{r-R}{\Delta/2}\right) & R - \frac{\Delta}{2} < r < R + \frac{\Delta}{2} \\ \pi & R + \frac{\Delta}{2} < r \end{cases} \tag{16}$$

This means that all links are equal to $\mathbf{1}$ except for the t-links in a single time-slice at fixed $t = 1$. The phase changes from 0 to π from inside to outside (or inverse). The graphs of $\alpha_\pm(r)$ for our largest lattice $40^3 \times 2$ is shown in the right diagrams of fig. 16. In our computations, R is set to half the lattice size, and Δ is chosen such that only 3 links along any direction are equal to $+\mathbf{1}$ and $-\mathbf{1}$, respectively. The colour vector $\vec{n}$ changes according to the spatial direction (see fig. 13).

2. The orientable vortex is constructed in a similar way:

$$U_\mu(x^\nu) = \begin{cases} \exp\left(\mathrm{i}\alpha(r)\,|n_k|\,\sigma_k\right) & t = 1,\ \mu = 4 \\ \mathbf{1} & \text{else} \end{cases} \tag{17}$$

$$|n_k| = |x_k|\,/r, \vec{r} = (x, y, z). \tag{18}$$

Due to the absolut value of the coordinates which enter the definition, the orientable vortex is symmetric in x, y and z, in distinction to the non-orientable vortex.

The distinction non-/orientable refers to the orientation of the vortex surface assigned by abelian projection. While the orientable vortex has a global orientation, the non-orientable vortex consists of 2 patches of opposite orientation separated by a closed monopole worldline. The position of this worldline which can be determined in maximal abelian gauge depends on the U(1) subgroup which is chosen for the gauge and the projection. In fig. 14 the loops corresponding to the σ_1, σ_2 and σ_3 subgroups are depicted.

The fundamental difference between an orientable and a non-orientable vortex can be understood by considering the vector field $\vec{n}$, which parametrizes the direction of the links in colour space (see fig. 14). The orientation of a point in abelian projection is obtained by taking the sign of the z-component of the local $\vec{n}$-vector. Prior to that, one can however perform a gauge transformation in order to align all vectors along the positive or negative z-direction. For a non-orientable vortex, this is not possible by a continuous transformation.

For a spherical vortex alone, the topological charge measured on the unsmoothed links is vanishing, since only the $U_{t\alpha}, \alpha = x, y, z$ plaquettes are non-zero, which gives a zero

$$Q \sim \epsilon_{\mu\nu\rho\sigma} U_{\mu\nu} U_{\rho\sigma} \tag{19}$$

This is independent of the lattice constant and thus holds also in the continuum limit. For the orientable vortex, the topological charge after cooling and the overlap index are also equal to 0, in keeping with the continuum expectation.

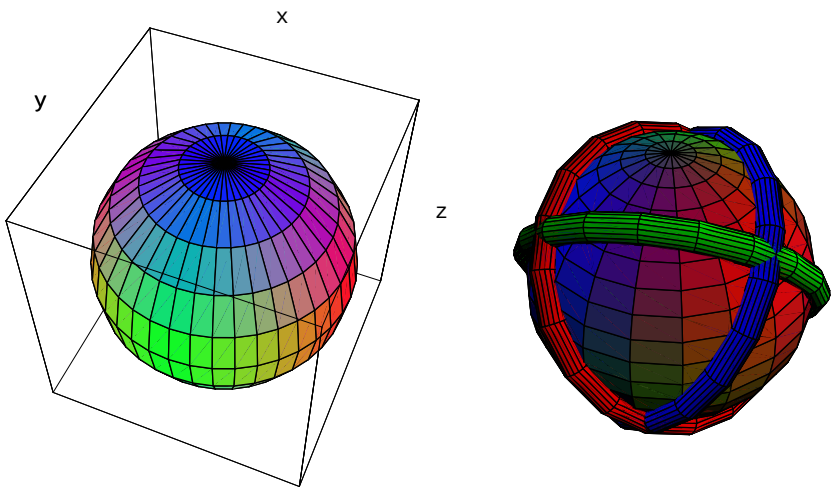

Figure 14. Non-orientable vortex surface (l) leads to monopole lines after abelian projection (r)

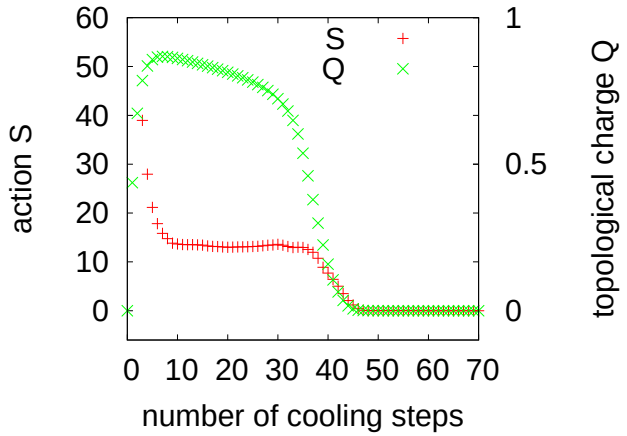

Figure 15. First, during cooling topological charge rises to ± 1 for $\alpha_\pm$ while the action S reaches a (non-zero) plateau

However, we find a discrepancy in the case of the non-orientable sphere vortex. First, during cooling the topological charge rises near to ± 1 for $\alpha_\pm$ (fig. 15).

Further, the index of the overlap operator is also non-zero, $\mathrm{ind}D = \pm 1$ for $\alpha_\pm$. Details are given in the table below:

type	n_+	n_-	$\mathrm{ind}D = n_- - n_+$
non-orientable, α_-	3	4	1
non-orientable, α_+	1	0	-1
orientable, $\alpha_\pm$	0	0	0

The scalar density of the fermionic zeromodes is shown in fig. 16, along with the phase of the links. It appears that the fermions avoid regions with large link angles, or better, large Polyakov lines (which is a gauge-invariant quantity).

The non-orientable vortex also gives extra contributions to the index when it is combined with other vortices, possibly including intersection points which produce "real" topological charge.

More generally, the following empirical rule can be formulated: a non-orientable sphere vortex contributes to cooled topological charge and Dirac operator index with an integer given by the "winding number" of the links. To compute this "winding number", the t-links are seen as a map not from $\mathbf{T}^4$, but from the compactified time-slice $t = 1$, in which the sphere is located, to SU(2). The time-slice can be compactified to S^3 because the links outside the sphere are all equal to $+\mathbf{1}$.

The discrepancy between overlap index and continuum topological charge is not due to the coarse discretization. We have used lattice sizes with $N_t = 2$ and N_s ranging from 8 to 40 in steps of 4.

The reason for the seeming contradiction is the singular nature of the continuum gauge field corresponding to a spherical vortex. This singularity invalidates the usual derivation of the index theorem.

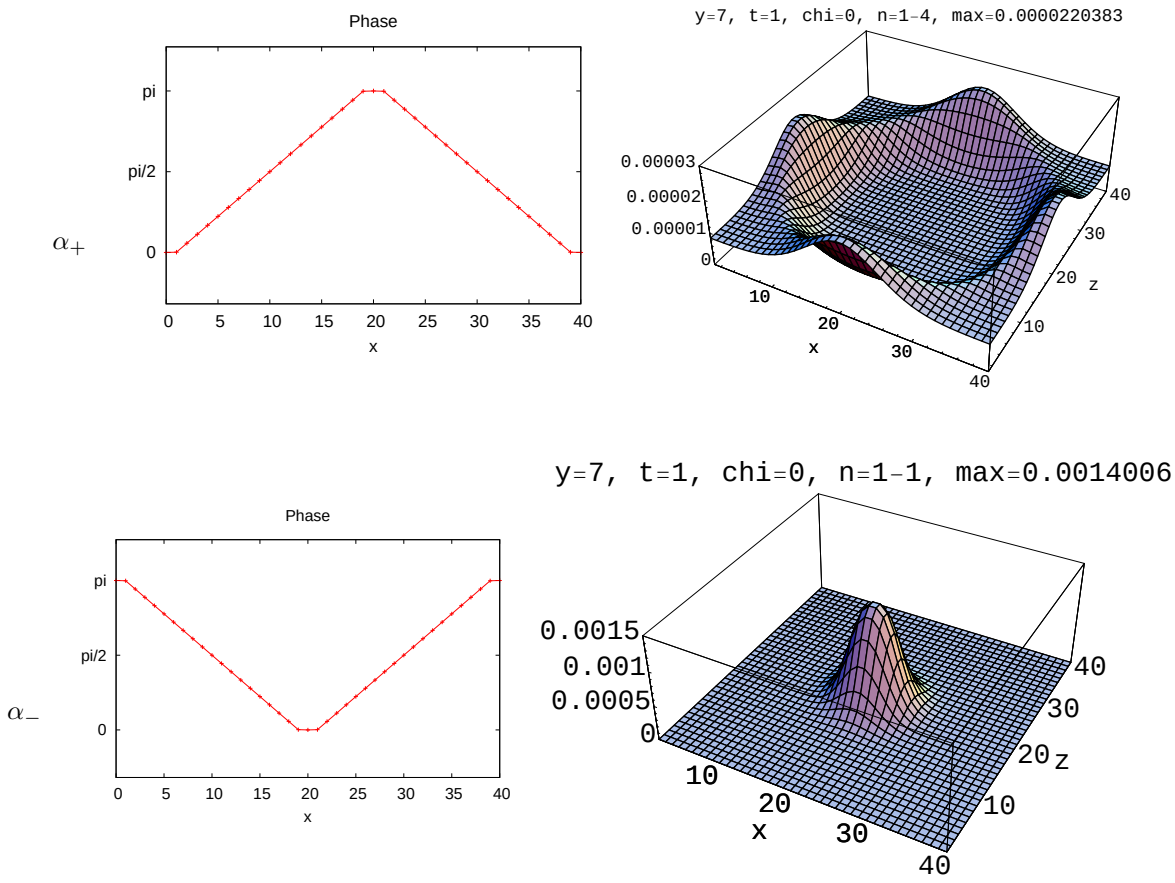

Figure 16. α_+- resp. α_--link phase-diagrams with corresponding scalar density of the fermionic zeromodes.

3.2 Investigation of near-zero modes of the Dirac operator

It is an interesing question whether the failure to explain the chiral condensate from center projected configurations is caused by the approximation which is due to the chirally improved fermions or whether pure P-vortices miss some important information concerning chiral symmetry breaking. This can be compared to the determination of the topological charge, where orientation information of the vortices is important for the determination of the topological charge. First we will again use the overlap Dirac operator which is obeying the Ginsparg-Wilson relation. Therefore the eigenvalues lie on the Ginsparg-Wilson circle, a circle with radius $1/2$ and center $(1/2, 0)$ in complex plane. Some results of these eigenvalues are shown in fig. 17.

The results for overlap fermions agree with those for chirally improved fermions [27, 28]. However we find a different behaviour for staggered fermions. The Dirac operator for massless staggered fermions χ reads:

$$D_{sf} = \frac{1}{2a} \sum_{\mu} \eta(x,\mu) P(x,\mu) \tag{20}$$

with $P(x,\mu) = \big[U(x,\mu)\chi(x+a_\mu) - U^\dagger(x-a_\mu,\mu)\chi(x-a_\mu)\big]$.
$\eta(x,\mu) = (-1)^{\sum_{\nu(<\mu)} x_\nu}$ are the staggered fermion phases. Its eigenvalues are imaginary and an example for a spectrum is shown in fig. 18.

We don't see any gap in center projected and vortex removed configurations in contradiction to overlap and chirally improved fermions. The gaps reappear again for vortex removed configurations if we use antiperiodic boundary conditions (see fig. 19).

4 Conclusion

To conclude we summarize the main facts of Center Vortex investigations:

- Confining Disorder $\equiv$ Center Disorder, caused by center vortices.
- P-vortices locate center vortices $W_n/W_0 = (-1)^n$

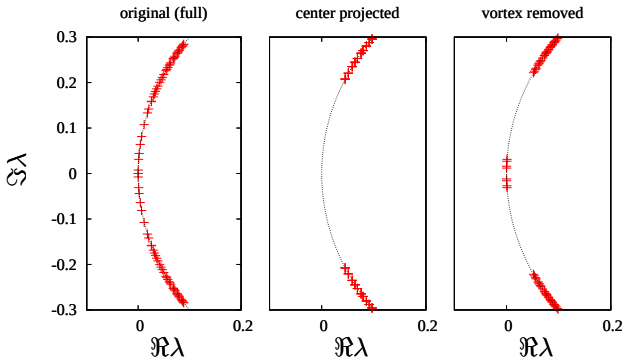

Figure 17. Eigenvalues of the Overlap Dirac operator

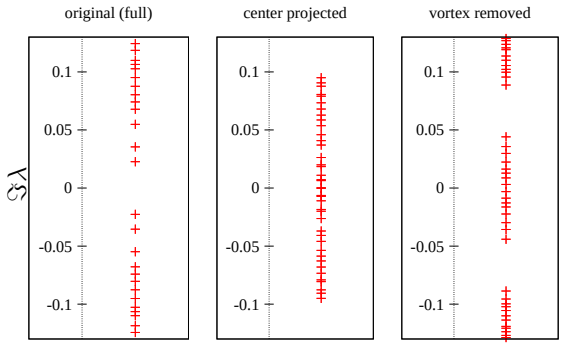

Figure 18. Eigenvalues of the Staggered Fermion operator

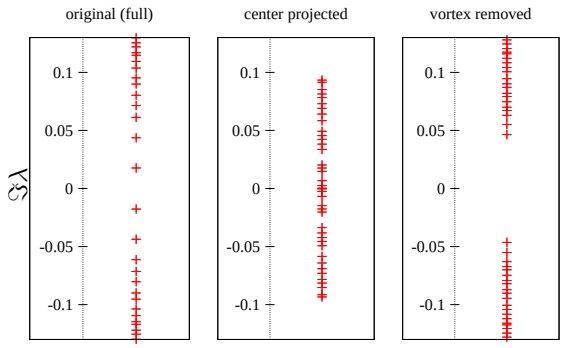

Figure 19. Eigenvalues of the Staggered Fermion operator for antiperiodic boundary conditions

- Center Dominance: The projected string tension is close to the asymptotic string tension σ of full Monte-Carlo configurations $\chi_{cp}(R,R) \approx \sigma$ $(R \geq 2)$
- Vortex density shows asymptotic scaling.
- Upon abelian projection, center vortices appear as chains of monopoles and antimonopoles.
- In the deconfined phase, vortices are static.They are composed of space-space plaquettes. They are orientable and have the topology of a torus.
  (Polyakov loop behaviour)
- In the confined phase P-vortices are unorientable.
- Pontryagin index from vortex intersection and writhing points
- Topological susceptibility mainly from writhing points
- Vortex removal restores chiral symmetry
- Index theorem fulfilled for U(1) vortices
- Index theorem puzzeling for SU(2) vortices
- Discrepancy between staggered and overlap fermions for P-vortices

References

[1] M.Creutz, Phys.Rev. **D21**, 2308 (1980).
[2] G.S.Bali, K.Schilling, C.Schlichter, Phys.Rev. **D51**, 5165 (1995).
[3] T.A.DeGrand, A.Hasenfratz, T.G.Kovacs, Nucl.Phys.Proc.Suppl. **63**, 528 (1998).
[4] A.S.Kronfeld, G.Schierholz, U.J.Wiese, Nucl.Phys. **B293**, 461 (1987).
[5] T.Suzuki I.Yotsuyanagi, Phys.Rev. **D42**, 4257 (1990).
[6] L.Del Debbio, M.Faber, J.Greensite, and S.Olejnik, Phys.Rev. **D53**, 5891 (1996).

[7] G.'t Hooft, Nucl.Phys. **B138**, 1 (1978).
[8] G.Mack, V.B.Petkova, Ann.Phys. **123**, 442 (1979).
[9] J.M.Cornwall, Nucl.Phys. **B157**, 392 (1979).
[10] L.Del Debbio, M.Faber, J.Greensite, and S.Olejnik, Phys.Rev. **D55**, 2298 (1997).
[11] C.Alexandrou, P.de Forcrand, M.D'Elia, Nucl.Phys. **A663**, 1031 (2000).
[12] P.de Forcrand, M.Pepe, Nucl.Phys. **B598**, 557 (2001).
[13] K.Langfeld, H.Reinhardt, A.Schäfke, Phys.Lett. **B504**, 338 (2001).
[14] M.Faber, J.Greensite, S.Olejnik, JHEP **11**, 053 (2001).
[15] K.Langfeld, H.Reinhardt, O.Tennert, Phys.Lett. **B419**, 317 (1998).
[16] K.Langfeld, O.Tennert, M.Engelhardt, H.Reinhardt, Phys.Lett. **B452**, 301 (1999).
[17] M.N.Chernodub, M.I.Polikarpov, A.I.Veselov, M.A.Zubkov, Nucl.Phys.Proc.Suppl. **73**, 575 (1999).
[18] R.Bertle, M.Faber, J.Greensite, S.Olejnik, JHEP **03**, 019 (1999).
[19] M.Faber, J.Greensite, S.Olejnik, Phys.Rev. **D57**, 2603 (1998).
[20] G.Mack, H.Meyer, Nucl.Phys. **B200**, 249 (1982).
[21] H.Meyer, Nucl.Phys. **B235**, 115 (1984).
[22] R.Bertle, M.Faber, in *Quark Confinement and the Hadron Spectrum V*, (ed. N.Brambilla and G.M.Prosperi, World Scientific, Singapore, 2003), pp. 3-12 [hep-lat/0212027].
[23] K.Langfeld, hep-lat/0212032.
[24] R.Bertle, M.Faber, J.Greensite, S.Olejnik, Phys.Rev. **D69**, 014007 (2004).
[25] P.de Forcrand, M.D'Elia, Phys.Rev.Lett. **82**, 4582 (1999).
[26] H.Reinhardt, O.Schroeder, T.Tok, V.C.Zhukovsky, Phys.Rev. **D66**, 085004 (2002).
[27] S.Solbrig *et. al.*, PoS LAT2005, 301 (2005) [hep-lat/0509052].
[28] J.Gattnar *et. al.*, Nucl.Phys. **B716**, 105 (2005).
[29] P.H.Ginsparg, K.G.Wilson, Phys.Rev. **D25**, 2649 (1982).
[30] M.Lüscher, Phys.Lett. **B428**, 342 (1998).
[31] H.Neuberger, Phys.Rev. **D57**, 5417 (1998).
[32] H.Neuberger, Phys.Lett. **B427**, 353 (1998).
[33] C.Gattringer, Phys.Rev. **D63**, 114501 (2001).
[34] C.Gattringer, I.Hip, C.B.Lang, Nucl.Phys. **B597**, 451 (2001).
[35] J.M.Cornwall, Phys.Rev. **D58**, 105028 (1998).
[36] J.M.Cornwall, Phys.Rev. **D61**, 085012 (2000).
[37] M.Engelhardt, H.Reinhardt, Nucl.Phys. **B585**, 591 (2000).
[38] R.Bertle, M.Engelhardt, M.Faber, Phys.Rev. **D64**, 074504 (2001).